Disturbance observer-based torsional vibration damper for variable-speed wind turbines

Zhu, Hongzhong
Research Institute for Applied Mechanics

Yoshida, Shigeo
Research Institute for Applied Mechanics

出版情報：IFAC Journal of Systems and Control. 14, pp.100112-, 2020-12. Elsevier
バージョン：
権利関係：

Disturbance observer-based torsional vibration damper for variable-speed wind turbines

Hongzhong Zhu[a,*], Shigeo Yoshida[a]

[a]*Research Institute for Applied Mechanics, 6-1 Kasuga-koen, Kasuga 816-8580, Japan*

Abstract

This paper presents a robust torsional vibration damper for variable-speed wind turbines based on the disturbance observer method. The damper is designed by explicitly taking into account the pole placement of the closed-loop system with model uncertainties. Unlike the conventional band-pass filter method, it is analyzed that the proposed method not only has good performance on noise attenuation, but also can maintain the low-frequency gain of the drivetrain system. The performance of other generator speed-based controllers, such as the blade pitch controller, can be preserved without the retuning procedures. An experimental system having high consistency with a 2 MW wind turbine is developed and the real-time hardware-in-the-loop experiments are carried out to demonstrate the effectiveness of the damper.

Keywords: vibration reduction, structural flexibility, gearbox, wind turbine

1. Introduction

As the size of a wind turbine increases, large force and torque bring up the influence of the gearbox and other structural flexibilities in the overall turbine

*corresponding author, zhuhongzhong@riam.kyushu-u.ac.jp

dynamic response, which often leads to failure in the drivetrain components (Wang et al., 2018; Chen and Song, 2016). It was reported that gearbox-related failures are responsible for more than 20% of the downtime of wind turbines (Girsang et al., 2014). In addition, the torsional vibrations in rotor and drivetrain would also be transmitted to power grid system to cause the electrical power oscillations (Cheng et al., 2016).

In a fixed speed wind turbine, the generator acts as a strong damper, with the torque increasing rapidly with generator speed. Therefore, the torsional mode of the drivetrain is well damped. In a variable speed wind turbine operating at constant generator torque, however, the generator torque no longer varies with generator speed so that there is little damping from the generator. Although the structural damping in shafts and gearbox has some effects on the vibration reduction, it contributes only a small fraction of 1% of critical damping (Burton et al., 2011). Torsional damper can be accomplished by making use of the generator torque to provide an additional damping torque having opposite phase with the generator speed, i.e., by band-pass filter (Bossanyi, 2000) or state feedback method (Licari et al., 2013). The methods attract much attention for their simplicity and intuitiveness, however, it will be shown in this study that the drivetrain characteristics in low-frequency domain would be changed, and the performance of other controllers, such as the blade pitch controller, might be degraded. A study on torsional resonance mitigation using a virtual inertia was performed in (Girsang et al., 2013). The virtual inertia is activated when the system is under resonant and switched off in other cases. The on-off behavior would cause rapid change in the torque, which could cause detrimental impacts to the

system. A nonlinear torsional damper based on sliding mode control theory was proposed in (Fateh et al., 2017) based on a high-order drivetrain model. The effects caused by the signal preprocessing step, such as the high-pass filter to remove the dc component of the generator speed, are not taken into account during the design, which may deteriorate the stability of the system. Recently, a method utilizing the speed difference information between the generator and the wind turbine rotor was studied in (Kambrath et al., 2018). The method requires an additional speed sensor, which may not be available in practical situation.

In motion control community, vibration suppression for mechanical systems has been extensively studied. Many methods, such as the polynomial method (Manabe, 2003) and observer-based methods (Hori et al., 1999; Ji and Sul, 1995), have been proposed to improve the rigidity of the system. Disturbance observer (DOB) is one of these methods that is well-known for its simplicity and superior performance, and has been implemented in many mechanical systems (Sariyildiz and Ohnishi, 2015). A method using the disturbance observer combined with a second order band-pass filter has been proposed for drivetrain vibration reduction in (Zhu et al., 2017). The parameters of the second order band-pass filter are determined by solving a constraint convex optimization problem. Although the effectiveness of the method has been demonstrated by simulation and experiments, the robustness of the method in the presence of model uncertainties has not been explicitly discussed. Besides, in their experiments, the flexibility of the drivetrain was implemented numerically by a digital signal processor (DSP), and therefore the effects of some physical phenomena, such as the mechanical friction

and the model uncertainties, would not be properly evaluated.

To extend the study of (Zhu et al., 2017), a new DOB-based damping method combined with a general form band-pass filter is proposed. By the method, a higher degree of design freedom can be obtained and more design specifications are possible to be achieved. Concretely, the robustness of the damper against the model uncertainties as well as the stability of the system are taken into account and expressed by linear matrix inequality (LMI) approach, and the damper design problem results in solving an optimization problem. Moreover, it is proved in this study that the disturbance observer-based method can maintain the low-frequency gain of the system so that the performance of other controllers, such as the blade pitch controller, can be preserved without the retuning procedure. A real-time hardware-in-the-loop experimental system whose characteristics are very close to a 2 MW wind turbine is developed to implement and verify the proposed method.

The remainder of this paper is given as follows. As a preliminary, a wind turbine model and conventional band-pass filter method are firstly introduced in Section 2. Then, the proposed method and its properties are presented in Sections 3 and 4, respectively. Finally, the hardware-in-the-loop experiments and the experimental results are discussed in Section 5.

2. Wind Turbine Model and Conventional Vibration Damper

2.1. Aerodynamic Model

Wind turbines are complex mechanical systems immersed in three dimensional wind field. Suppose that the rotor of a wind turbine is capable to follow the wind direction and the oncoming wind is steady, the aerodynamic

torque T_R can be expressed by (Bianchi et al., 2007)

$$T_R = \frac{1}{2}\rho\pi R^3 \frac{C_p(\lambda,\beta)}{\lambda} v^2, \tag{1}$$

where v is the wind speed, ρ the air density, R the rotor-plane radius, β the pitch angle of blades, λ the tip-speed ratio defined as the ratio between the tangential speed of the tip of a blade and the wind speed. The term C_p is the power coefficient defined as the ratio between the power captured by a wind turbine and the total upstream wind power flowing into the rotor plane. The coefficient C_p is a function of the pitch angle β and the tip-speed ratio λ, and often obtained as a look-up table by steady state simulation, e.g., with Bladed (Bossanyi, 2015).

Note that the oncoming wind is normally unsteady, the angle of attack of the airfoil elements of the blades is continuously changing and so the instantaneous torque cannot be determined via the equation (1). This is because the aerodynamic force on the airfoil elements are not in phase with the angle of attack in a continuously changing situation. As the aerodynamic torque is an external input and would not affect the stability of the wind turbine control system, the unsteady situation is not considered in this study in common with other research on wind turbine control, such as (Boukhezzar et al., 2007; Licari et al., 2013; Bianchi et al., 2007).

2.2. Generator Model

A permanent-magnet synchronous machine (PMSM) is considered to be applied as the generator. For a symmetrical 3-phase smooth-air-gap PMSM with sinusoidally-distributed windings, its mathematical model can be de-

scribed by (Yin et al., 2007)

$$\frac{d}{dt}i_d = -\frac{R_s}{L_d}i_d + \omega_e\frac{L_q}{L_d}i_q + \frac{1}{L_d}v_d, \tag{2}$$

$$\frac{d}{dt}i_q = -\frac{R_s}{L_q}i_q - \omega_e\frac{L_d}{L_q}i_d - \omega_e\frac{\phi_e}{L_q} + \frac{1}{L_q}v_q, \tag{3}$$

$$T_G = \frac{3}{2}n_p[\phi_e i_q + (L_d - L_q)i_d i_q], \tag{4}$$

where i and v are the current and voltage, respectively, L the self-inductance, R_s the stator resistance, ω_e the electrical rotating speed, n_p the number of pole pairs, ϕ_e the permanent magnetic flux, and T_G the electromagnetic torque. The subscripts $_d$ and $_q$ refer to the physical quantities in rotating reference frame via Park transformation.

Proportional-integral (PI) current regulator with pole-zero cancellation feature (Zhu and Fujimoto, 2014) is applied for generator current control. The $d-$axis current i_d is regulated to be zero so that the generator torque is proportional to the $q-$axis current, as given by the equation (4). The $q-$axis current demand i_q^d is calculated from the generator torque demand T_G^d that

$$i_q^d = T_G^d/K_t, \tag{5}$$

where K_t is the torque coefficient assigned by $K_t = \frac{3}{2}n_p\phi_e$. By the method, the transfer function from the torque demand to the generated torque becomes the first-order system expressed by

$$\frac{\Gamma_G(s)}{\Gamma_G^d(s)} = \frac{1}{Ts+1}, \tag{6}$$

where s is the Laplace operator, Γ_G and Γ_G^d are the Laplace transform of T_G and T_G^d, respectively. The parameter T is the time constant determined by the parameters of the PI controller. The generator current control is usually

high-bandwidth (T is small) and therefore the torque demand T_G^d is regarded as T_G, i.e., $T_G^d \approx T_G$, in the following analysis.

2.3. Drivetrain Model

As the size of a wind turbine increases, the flexibility associated with the rotor structure also increases. In terms of controller design, a two-mass model with shaft flexibilities or a three-mass model representing both shaft flexibilities and blade bending dynamics are often adopted for reducing the complexity (Burton et al., 2011; Licari et al., 2012, 2013). For ease of comprehension, a two-mass model is employed for this study. The damper based on a three-mass model is discussed in the Appendix.

In a two-mass model ignoring the blade bending dynamics and the nonlinear mechanical frictions, the motion equations can take the form of

$$J_R\dot{\omega}_R + D_S\left(\omega_R - \omega_G\right) + K_S\theta_S = T_R, \tag{7}$$

$$J_G\dot{\omega}_G - D_S\left(\omega_R - \omega_G\right) - K_S\theta_S = T_G, \tag{8}$$

$$\dot{\theta}_S = \omega_R - \omega_G, \tag{9}$$

where J, ω and T represent the moment of inertia, the rotational speed and the torque, respectively. The subscripts $_R$ and $_G$ refer to the rotor-side quantities and the generator-side quantities, respectively. K_S is the representative gear stiffness, and D_S is the linear damping coefficients contributed by the gear and bearings. The term θ_S is the torsional angle. Note that the gear ratio is ignored for the sake of brevity and the rotor-side quantities (J_R, T_R, and ω_R) are expressed with respect to the generator shaft. Since the structural damping is small, the damping coefficient D_S is set as $D_S = 0$ for ease of analysis.

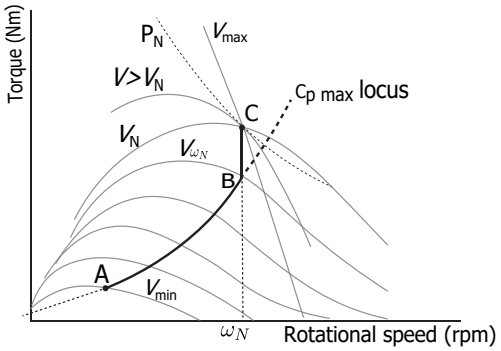

Figure 1: Control strategy of a wind turbine (Zhu et al., 2017).

By calculation, the transfer functions from T_R and T_G to ω_G are formulated by

$$\frac{\Omega_G}{\Gamma_R} = \frac{1}{J_G s}\frac{\omega_z^2}{s^2+\omega_p^2}, \tag{10}$$

$$\frac{\Omega_G}{\Gamma_G} = \frac{1}{J_G s}\frac{s^2+\omega_z^2}{s^2+\omega_p^2}, \tag{11}$$

where Ω_G, Γ_G and Γ_R are the Laplace transform of ω_G, T_G and T_R, respectively. The terms ω_p and ω_z are the resonant angular frequency and the anti-resonant angular frequency expressed by $\omega_p = \sqrt{\frac{K_S}{J_R}+\frac{K_S}{J_G}}$ and $\omega_z = \sqrt{\frac{K_S}{J_R}}$. From the *final value theorem*, the final value of the impulse response of $\frac{\Omega_G}{\Gamma_R}$ and $\frac{\Omega_G}{\Gamma_G}$ exists and converges to $\frac{1}{J_G+J_R}$ when the structural damping is considered in (10) and (11).

2.4. Control Strategy

For a variable-speed pitch-regulated wind turbine, the basic control objectives are to maximize the energy capture at low wind speeds whereas to limit the aerodynamic power at above-rated wind speeds. Fig. 1 depicts the basic control strategy on the torque-rotational speed plane.

In low wind speeds, the pitch angle of the blades is set at the fine value ($\beta = 0$) and the rotor speed is controlled to keep the tip-speed ratio, λ, at its optimal value. The turbine is operated along the optimal locus with the highest power efficiency ($C_{p_{\max}}$ locus in Fig. 1 between the point A and B). The torque reference $\tilde{T}_G$ is given by

$$\tilde{T}_G = K_t \omega_G^2, \tag{12}$$

where K_t is a scalar determined by $C_{p_{\max}}$ (Burton et al., 2011). At point B, the rotation speed arrives to its rated rotational speed ω_N at wind speed V_{ω_N}. The rotational speed is regulated at this value along the segment BC as wind speed increases from V_{ω_N} to the rated wind speed V_N.

In above-rated wind speeds, the torque reference for the generator is set as constant and the pitch angle of the blades is adjusted (pitch-to-feather) to shed the aerodynamic power and to let the wind turbine operate at the point C.

2.5. Conventional Band-pass Filter

A common approach to reduce the torsional vibration of drivetrain is to use a band-pass filter (Bossanyi, 2003)

$$G_f(s) = G \frac{2\zeta_b \omega_b s(1 + \tau s)}{s^2 + 2\zeta_b \omega_b s + \omega_b^2} \tag{13}$$

acting on the generator speed to generate the damping torque. The term ω_b should be close to the resonant angular frequency ω_p. ζ_b is set small to give a frequency response with narrow peak to avoid causing detrimental effect to the overall performance. The term $(1 + \tau s)$ is used to compensate for time-lags introduced during the speed measurement. The block diagram of

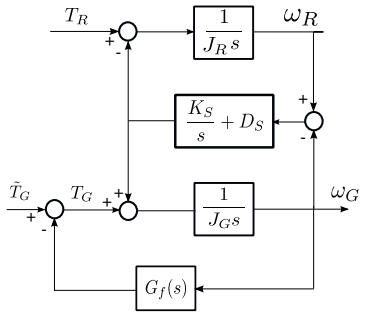

Figure 2: Conventional torsional vibration reduction method based on band-pass filter.

the method is shown in Fig. 2. For ease of analysis, the compensation term $(1 + \tau s)$ is ignored in the following.

By calculation, the transfer functions from T_R and $\tilde{T}_G$ to ω_G become

$$\frac{\Omega_G}{\Gamma_R} = \frac{\omega_z^2}{J_G s} \frac{s^2 + 2\zeta_b \omega_b s + \omega_b^2}{P_f(s)}, \tag{14}$$

$$\frac{\Omega_G}{\tilde{\Gamma}_G} = \frac{s^2 + \omega_z^2}{J_G s} \frac{s^2 + 2\zeta_b \omega_b s + \omega_b^2}{P_f(s)}, \tag{15}$$

where $\tilde{\Gamma}_G$ is the Laplace transform of $\tilde{T}_G$ and the term $P_f(s)$ in the denominator is expressed as

$$P_f(s) = s^4 + 2\zeta_b \omega_b s^3 + \left(\omega_b^2 + \omega_p^2 + G\frac{2\zeta_b \omega_b}{J_G}\right) s^2 + 2\zeta_b \omega_b \omega_p^2 s + \left(\omega_b^2 \omega_p^2 + \omega_z^2 G \frac{2\zeta_b \omega_b}{J_G}\right). \tag{16}$$

From (14) and (15), it can be analyzed that the final value of their impulse response is $\frac{1}{J_G + J_R} \frac{1}{1 + G\frac{\omega_z^2}{\omega_p^2}\frac{2\zeta_b}{J_G \omega_b}}$, which is smaller than the original two-mass model (10) and (11). Therefore, the low-frequency gain of the drivetrain system from the aerodynamic torque to the generator speed is reduced. As it will be shown in Section 4 and Section 5, this would deteriorate the performance of blade pitch controller on regulating the generator power since

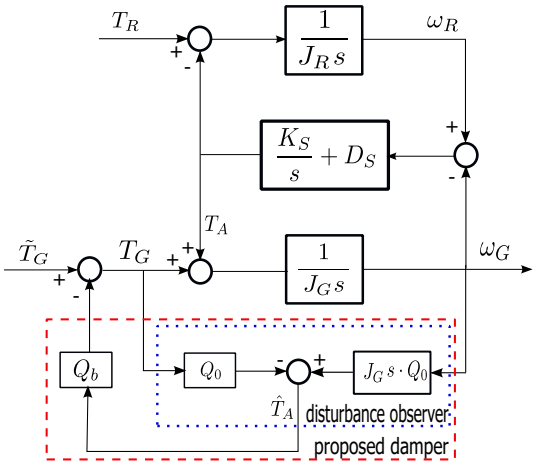

Figure 3: Disturbance observer-based damper (Zhu et al., 2017).

the sensitivity of the blade pitch to the generator speed is reduced.

3. Disturbance Observer-Based Vibration Damper

The disturbance observer-based damper was initially proposed in (Zhu et al., 2017), and the block diagram is shown within the dashed line in Fig. 3. In the figure, Q_0 is a low-pass filter, T_A is the drive torque transmitted from gearbox to the generator shaft and $\hat{T}_A$ is the estimation of T_A. The term Q_0 is chosen to provide a good balance between the noise attenuation and the estimation performance. The standard form of the disturbance observer is to apply the estimated signal $\hat{T}_A$ to feedback directly. By this manner, it will be shown that the control output ω_G becomes insensitive to the aerodynamic torque, which would invalid the blade pitch controller on power regulation since the generator speed is also insensitive to the wind speed.

To avoid the problem, a term Q_b is applied to filter the signal $\hat{T}_A$, as shown in Fig. 3. Defining Q as the multiplication of Q_0 and Q_b that $Q = Q_0 Q_b$, the

transfer functions from $\tilde{T}_G$ and T_R to ω_G becomes

$$\frac{\Omega_G}{\Gamma_R} = \frac{\omega_z^2 \cdot (1-Q)}{J_G s \cdot P(s)}, \tag{17}$$

$$\frac{\Omega_G}{\tilde{\Gamma}_G} = \frac{s^2 + \omega_z^2}{J_G s \cdot P(s)}, \tag{18}$$

where $P(s)$ is given as

$$P(s) = (s^2 + \omega_p^2)(1-Q) + (s^2 + \omega_z^2)Q. \tag{19}$$

It is observed that if $Q \approx 1$, which means that the original disturbance observer with a high-bandwidth low-pass filter is applied, the transfer functions (17) and (18) become $\frac{\Omega_G}{\tilde{\Gamma}_G} \approx \frac{1}{J_G s}$ and $\frac{\Omega_G}{\Gamma_R} \approx 0$. This implies that the system becomes rigid and the generator speed is insensitive to the aerodynamic torque, which should be avoided. In the following, Q is designed by considering the torsional vibration reduction and the preservation of the low-frequency gain of the systems (17) and (18).

3.1. General Form of Q

In the previous study in (Zhu et al., 2017), the filter Q is specified to be a second order band-pass filter, and the degree of design freedom may not be enough when considering the robustness of the damper against the model uncertainties. Therefore, a general form of Q having more design flexibility is required. In order to maintain the drivetrain characteristics at low-frequency domain, it is easy to see that the filter $Q(s)$ should have at least one zero at $s = 0$, i.e., $Q(0) = 0$, to let

$$\lim_{s \to 0} s \frac{\Omega_G}{\tilde{\Gamma}_G} = \frac{1}{J_G + J_R}. \tag{20}$$

Based on this consideration and taken into account the stability of the drivetrain system, $Q(s)$ should be designed subject to the following constraints

- $Q(s)$ has a zero at $s = 0$,
- $Q(s)$ has at least one relative degree for the implementation of the disturbance observer,
- $Q(s)$ has all poles in the left half of the s-plane, and
- $\frac{1}{P(s)}$ has all poles in the left half of the s-plane.

A general form of $Q(s)$ is considered as follows:

$$Q(s) = \frac{B(s)}{A(s)} = \frac{b_{n-1}s^{n-1} + b_{n-2}s^{n-2} + \cdots + b_1 s}{s^n + a_{n-1}s^{n-1} + \cdots + a_0}, \tag{21}$$

where $n \in \mathbb{N}$ ($n \geq 2$) is the degree of Q. The condition $a_0 \neq 0$ is required in (21) by the first constraint.

Substituting $Q(s)$ into the equation (19), the characteristic polynomial of $\frac{1}{P(s)}$ can be written as

$$P_N(s) = (s^2 + \omega_p^2)A(s) + (\omega_z^2 - \omega_p^2)B(s). \tag{22}$$

According to the *pole placement-polynomial approach* (Goodwin et al., 2001), $P_N(s)$ can be arbitrarily specified by $A(s)$ and $B(s)$ with the degree $n = 3$. The desired polynomial of $P_N(s)$ can be assigned as

$$P_{N_d}(s) = (s + p)\Pi_{i=1}^{2}(s^2 + 2\zeta_i\omega_i s + \omega_i^2) \tag{23}$$

with proper values of p, ζ_i and ω_i ($i = 1, 2$). Since the poles of $Q(s)$ are also introduced to the closed-loop system, as shown in (17), the stability criterion and the vibration mode of Q should be taken into account during the determination of p, ζ_i and ω_i.

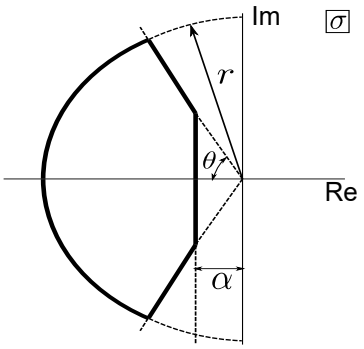

Figure 4: Region $\mathcal{S}(\alpha, r, \theta)$ for pole placement.

3.2. Design of Q with Model Uncertainties

In practical situation, the parameters, such as the moment of inertia of the drivetrain and the stiffness of the gearbox, are usually not known exactly and may vary across the years. Moreover, the resonant frequency of the system also varies under different wind conditions (Bir and Jonkman, 2007). Therefore, the model uncertainties should be considered during the design of $Q(s)$.

Suppose that the poles of $Q(s)$ and $\frac{1}{P(s)}$ are required to be in a region such that

$$\mathcal{S}(\alpha, r, \theta): \begin{cases} Re(\sigma) \leq -\alpha < 0, \\ |\sigma| \leq r, \\ \tan\theta \, \mathrm{Re}(\sigma) \leq -|\mathrm{Im}(\sigma)|, \end{cases} \tag{24}$$

as shown in Fig. 4. Confining the poles to this region ensures a minimum decay rate α, a maximum natural frequency (undamped) $\omega_d = r\sin\theta$ and a minimum damping ratio $\zeta = \cos\theta$. The requirement yields the constraints

(Chilali and Gahinet, 1996):

$$\begin{cases} A_Q X + X A_Q^T + 2\alpha X < 0, \\ \begin{bmatrix} -rX & A_Q X \\ X A_Q^T & -rX \end{bmatrix} < 0, \\ \begin{bmatrix} \sin\theta(A_Q X + X A_Q^T) & \cos\theta(A_Q X - X A_Q^T) \\ \cos\theta(X A_Q^T - A_Q X) & \sin\theta(A_Q X + X A_Q^T) \end{bmatrix} < 0, \end{cases} \tag{25}$$

and

$$\begin{cases} A_C Y + Y A_C^T + 2\alpha Y < 0, \\ \begin{bmatrix} -rY & A_C Y \\ Y A_C^T & -rY \end{bmatrix} < 0, \\ \begin{bmatrix} \sin\theta(A_C Y + Y A_C^T) & \cos\theta(A_C Y - Y A_C^T) \\ \cos\theta(Y A_C^T - A_C Y) & \sin\theta(A_C Y + Y A_C^T) \end{bmatrix} < 0, \end{cases} \tag{26}$$

where A_Q and A_C are the system matrices of $Q(s)$ and $\frac{1}{P(s)}$, respectively. $X \in \mathbb{S}^{n\times n}$ and $Y \in \mathbb{S}^{(n+2)\times(n+2)}$ are positive definite matrices.

Assuming that ω_p^2 varies in the interval $[\omega_{p_a}^2,\ \omega_{p_b}^2]$, the design of $Q(s)$ leads to the problem

$$\begin{aligned} &\text{find:} \quad a_{n-1}, \cdots, a_0, b_{n-1}, \cdots, b_1, X, Y \\ &\text{subject to :} \\ &\quad \text{condition (25)}, \\ &\quad \text{condition (26) with } A_C = A_C(\omega_{p_a}^2), \\ &\quad \text{condition (26) with } A_C = A_C(\omega_{p_b}^2). \end{aligned} \tag{27}$$

In order to help on regulating the characteristic polynomial of $\frac{1}{P(s)}$, a cost

function is set for (27) and the optimization problem becomes

$$\begin{aligned} \underset{a_{n-1},\cdots,a_0,b_{n-1},\cdots,b_1,X,Y}{\text{minimize}} : \ & \|\mathcal{C}\left(P_N(s,\omega_{p_0}^2)\right) - \mathcal{C}(P_{N_d})\|_2, \\ \text{subject to :} & \\ & \text{conditions in (27)} \end{aligned} \tag{28}$$

where $\mathcal{C}(\mathcal{P})$ is the vector whose elements are the coefficients of the polynomial $\mathcal{P}$, P_{N_d} is the desired polynomial and $P_N(s,\omega_{p_0}^2)$ is the characteristic polynomial of $\frac{1}{P(s)}$ at its nominal value given by

$$P_N(s,\omega_{p_0}^2) = (s^2+\omega_{p_0}^2)A(s) + (\omega_z^2 - \omega_{p_0}^2)B(s)$$

with $\omega_{p_0}^2 = (\omega_{p_a}^2 + \omega_{p_b}^2)/2$. The constraint conditions in (28) can ensure the poles of $Q(s)$ and $\frac{1}{P(s)}$ be confined in the region $\mathcal{S}$ for any $\omega_{p_i}^2 \in [\omega_{p_a}^2,\ \omega_{p_b}^2]$. The proof is given as follows:

Suppose $\omega_{p_i}^2$ is expressed by

$$\omega_{p_i}^2 = \lambda_i\omega_{p_a}^2 + (1-\lambda_i)\omega_{p_b}^2, \quad (0 \le \lambda_i \le 1) \tag{29}$$

then, the following equation can be obtained:

$$A_C(\omega_{p_i}^2) = \lambda_i A_C(\omega_{p_a}^2) + (1-\lambda_i)A_C(\omega_{p_b}^2). \tag{30}$$

The equation (30) ensures the following inequality constraint

$$A_C(\omega_{p_i}^2)Y + YA_C(\omega_{p_i}^2)^T + 2\alpha Y < 0 \tag{31}$$

be satisfied since its left side is expressed by

$$\begin{aligned} A_C(\omega_{p_i}^2)Y + YA_C(\omega_{p_i}^2)^T + 2\alpha Y = & \\ \lambda_i \cdot \left(A_C(\omega_{p_a}^2)Y + YA_C(\omega_{p_a}^2)^T + 2\alpha Y\right) + & \\ (1-\lambda_i) \cdot \left(A_C(\omega_{p_b}^2)Y + YA_C(\omega_{p_b}^2)^T + 2\alpha Y\right), & \end{aligned}$$

Table 1: Specification of the used wind turbine model

Property	Value
Rated power output	2.0 MW
Rated rotor speed	2.15 rad/s
Rated wind speed	11.6 m/s
Rotor diameter	76 m
Moment of inertia of rotor J_R	758.61* kg $\cdot$m^2
Moment of inertia of generator J_G	53.04 kg$\cdot$m^2
Equivalent linear-spring constant K_{S_0}	7.24×10^5 * N$\cdot$m/rad
Gear ratio N	87.97
Natural frequency of 1st drivetrain torsion (free-free mode) ω_{p_0}	120.83 rad/s

* The quantities are with respect to the generator shaft.

which is a linear combination of the last two constraints in the problem (28). In the same way, two other constraints of (26) for $\omega_p^2 = \omega_{p_i}^2$ can be proved.

The optimization problem (28) is a specific non-linear non-convex problem and could be solved by FMINSDP (Thore, 2013). Note that the solution from Section 3.1 could be used as the warm start solution for the problem (28). The degree of Q can be set higher to increase the independent parameters to find a solution for (28).

4. Analysis

A 2-MW variable-speed pitch-regulated wind turbine given in Table 1 are applied for our analysis. The time-lag of the generator speed measurement

is set as $\tau = 0.005$. The parameters ζ_b and ω_b of the BPF method are assigned as $\zeta_b = 0.38$ and $\omega_b = \omega_{p_0}$, respectively, and the parameter G is chosen to maximize the damping of the system by root locus analysis. The resulted damping factors of the drivetrain system are around 0.19. Note that although a broader peak (large ζ_b) can be set for the BPF method to suppress the vibration, it may be detrimental to the overall performance of the wind turbine (Burton et al., 2011). For the DOB-based method, the degree of the filter Q is set as $n = 3$ and the objective damping factors (ζ_1 and ζ_2) are set as same as the damping factors of the BPF method for a fair comparison. The variation bound of ω_p^2 is set as $\pm 15\%\, \omega_{p_0}^2$. This setting would be sufficient for a practical large wind turbine according to the study in (Bir and Jonkman, 2007). The region $\mathcal{S}$ is designed to cover the poles of the BPF-based system, and properly specified by $\alpha = 5$, $\zeta = \cos\theta = 0.1$ and $r = 150$.

The *pole placement-polynomial approach* is applied to obtain an initial solution of Q, as explained in Section 3.1. Then, the code FMINSDP (Thore, 2013), which is based on the gradient-based NLP-solver: *'fmincon'* (MathWorks, 2020), is applied to solve the problem (28). The setting of the two methods and the properties of their resulted drivetrain system are concluded in Table 2. The filter Q designed by (28) becomes

$$Q(s) = \frac{34.06s^2 + 3.52e3s}{s^3 + 218.46s^2 + 1.61e4s + 8.67e5}. \tag{32}$$

The pole locus of the system (vibration modes) under the condition that ω_p^2 varies from 85% to 115% of its nominal value is shown in Fig. 5. The contour lines of damping factors are shown in radial dotted lines and the region $\mathcal{S}$ is bounded by the thick curve. Poles 1$\sim$4 are the poles of $\frac{1}{P(s)}$ and poles 5-6 are the poles of Q. It is obtained that the poles of the system under the

Table 2: Setting of Parameters

Method	Parameters	Resulted damping ratio [-], damped frequency [rad/s]
BPF	$G = 2.12 \times 10^3$, $\zeta_b = 0.38$, $\tau = 0.005$, $\omega_b = \omega_{p_0}$	$\zeta_1 = 0.18$, $\zeta_2 = 0.19$, $\omega_1 = 104.02$, $\omega_2 = 141.25$
DOB-based	$n = 3$, $p = 1.2\omega_{p_0}$, $\zeta_1 = \zeta_2 = 0.19$, $\omega_1 = \omega_2 = 0.8\omega_{p_0}$	$\zeta_1 = 0.17$, $\zeta_2 = 0.19$, $\zeta_3 = 0.45$, $\omega_1 = 83.44$, $\omega_2 = 121.31$, $\omega_3 = 76.11$

uncertainties are all confined in the designated region, which indicates that the problem (28) is properly solved. Note that the solution (32) is a local optimal solution since the solver *'fmincon'* is based on local optimization algorithms (MathWorks, 2020).

The characteristics of the transfer function $\frac{\Omega_G}{\tilde{\Gamma}_G}$ compared with the original two-mass model (11) are shown in Fig. 6. From the results, we can see that both of the methods can properly reduce the vibration mode since the peak at the natural frequency is reduced. However, as illustrated by the enlarged graph at the upper left side of the figure, the gain in low-frequency domain is slightly reduced by the BPF method whereas maintained by the DOB-based method. In order to discuss the effects of the dampers on the blade pitch regulation, the characteristics of the blade pitch control at over-rated wind speeds are also discussed. The aerodynamic model (1) is linearized at $\hat{v} = 13$ m/s, $\hat{\omega}_R = 2.15$ rad/s, and $\hat{\beta} = 6.5$ deg and the block diagram of the system is shown in Fig. 7. The blade pitch PI controller is properly set as

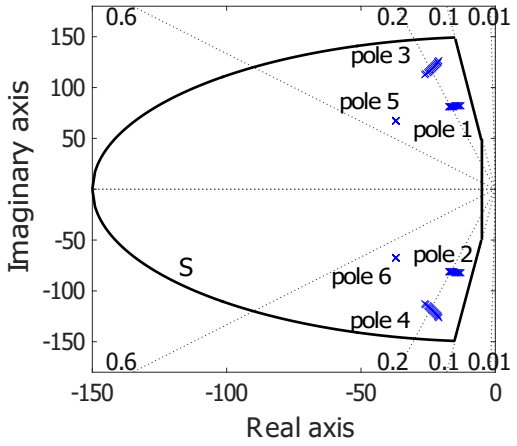

Figure 5: Poles locus (shown by '×') of the vibration modes when ω_p^2 varies from 85% to 115% of its nominal value $\omega_{p_0}^2$.

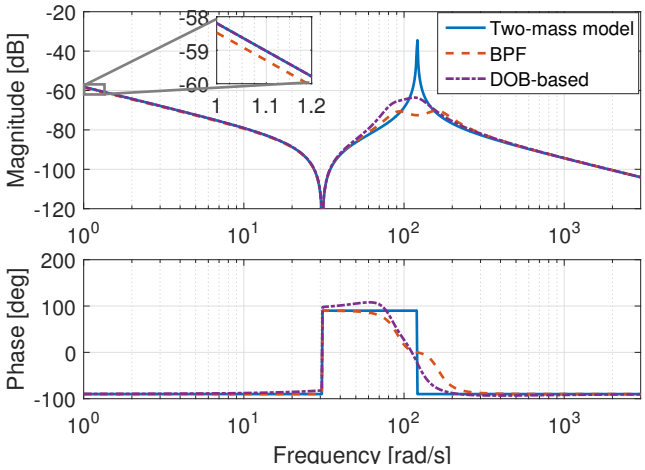

Figure 6: Characteristics of $\frac{\Omega_G}{\bar{\Gamma}_G}$ of the original two-mass model and the models with the vibration dampers. The solid line shows the original two-mass model. The dashed line and the dash-dotted line show the BPF method and the DOB-based method, respectively.

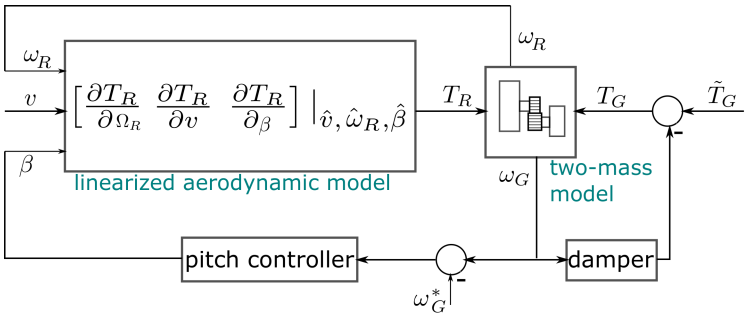

Figure 7: The block diagram of the linearized wind turbine model.

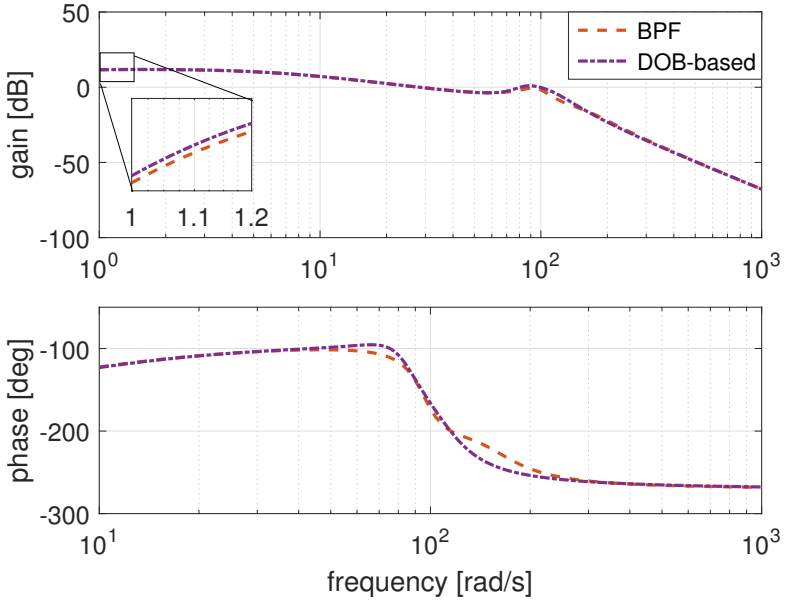

Figure 8: The characteristics of the linearized system from wind speed v to the blade pitch angle β.

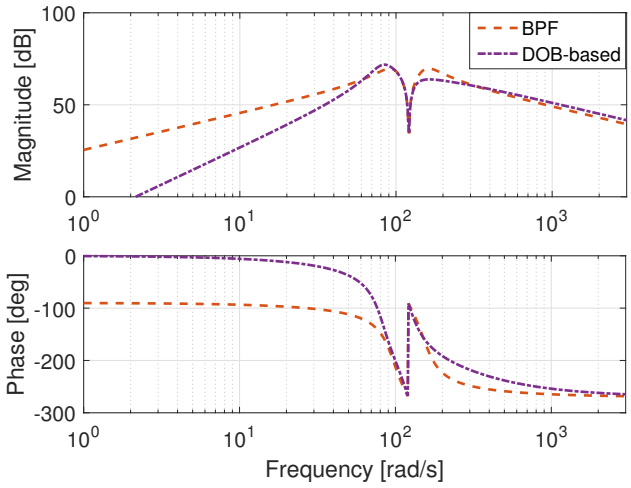

Figure 9: The characteristics of the sensitivity function of the closed-loop system with the dampers.

$K_p = 1.20$ and $K_i = 0.10$. Fig. 8 shows the characteristics of the blade pitch β with response to the wind speed v when the two dampers are applied. The low-frequency gain, as shown in the enlarged graph, is also slightly reduced by the BPF method, which means the response of the blade pitch would be slightly deteriorated. This will also be demonstrated by the experiment in Section 5.

To study the influence of the measurement noise on the generator torque, the characteristics of the control sensitivity (the transfer function from the measurement noise to the generator torque) are also studied, as shown in Fig. 9. A smaller gain means a better noise attenuation and the system would be more robust to the measurement noise. From the result, it can be found that a better noise rejection in low-frequency domain can be obtained by the DOB-based method.

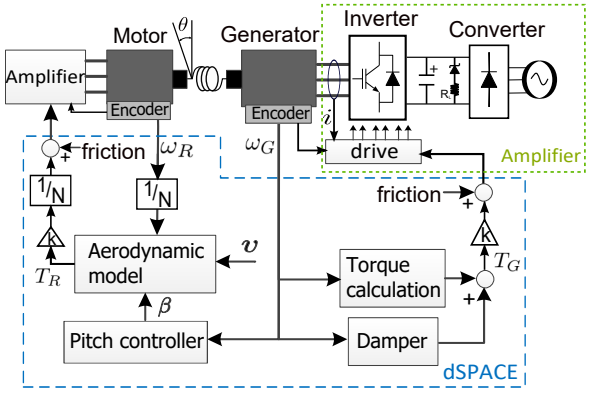

Figure 10: Configuration of experimental system.

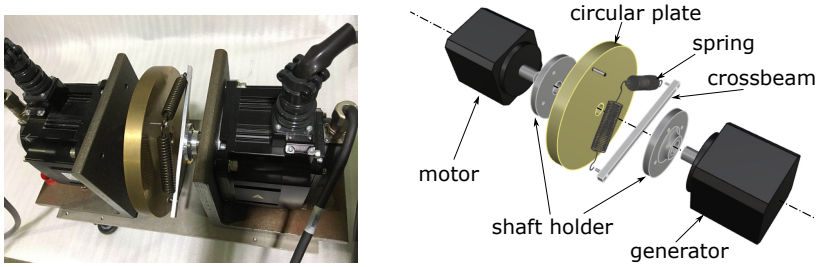

Figure 11: Motor-generator bench (left) and the construction (right).

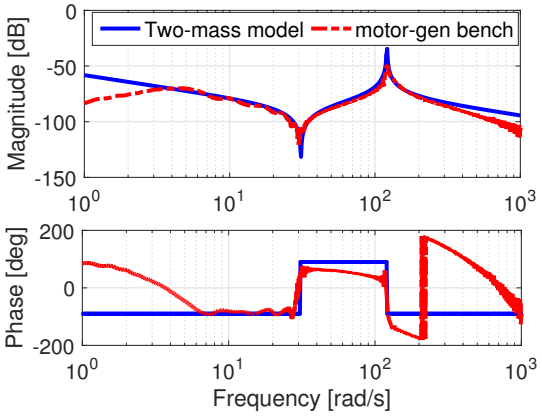

Figure 12: Characteristics of motor-generator bench (dashed line) and the ideal two-mass model.

5. Experiment

An experimental system consisting of a motor-generator bench (HG-SR102 by MITSUBISHI ELECTRIC®) and the DS1104 R&D controller board (developed by dSPACE®) is developed to evaluate the performance of the torsional vibration dampers and their effects on the blade pitch control. The configuration of the experimental system is shown in Fig. 10. The current controller of the motor and the generator is implemented in their servo amplifiers. The aerodynamic model, the pitch controller, the torque reference and the vibration dampers are implemented in the controller board. A motor-generator bench is applied to model the drivetrain dynamics, and the construction of the experimental system is shown in Fig. 11. A circular plate, which is fixed on the motor shaft by a shaft holder, is employed to adjust the moment of inertia of the motor. In order to let the experimental system have same characteristics with the aforementioned 2-MW wind turbine, the stiffness of the coupling system is determined as 21.8 Nm/rad, which is very low-rigidity and not commercially available in practical situation. In the experiments, therefore, a crossbeam with two tension springs are applied to form the coupling system. The crossbeam is fixed on the generator shaft and the springs are applied to tense the circular plate and the crossbeam, as shown in Fig. 11. By the mechanism, the stiffness of the system can be tuned by the length of crossbeam. The properties of the motor-generator bench are shown in Table 3.

To scale down the aerodynamic torque and the generator torque to an applicable level for the experimental system, a constant scalar $k = 5.03 \times 10^{-5}$ is applied. The Coulomb friction and viscous friction of the motor/generator

Table 3: Parameters of motor-generator bench

Property	value
Moment of Inertia of motor [kg·m^2]	2.29×10^{-2}
Moment of Inertia of generator [kg·m^2]	1.60×10^{-3}
Stiffness coefficient of coupling [Nm/rad]	21.83
Self-inductance L ($L_d = L_q$) [mH]	1.5
Stator resistance R_s [Ω]	0.54
Number of pole pairs n_p [-]	4
Torque constant K_t ($=\frac{3}{2}n_p\phi_e$) [Nm/A]	0.52

are compensated numerically, as shown in Fig. 10. The comparison of the characteristics between the experimental system and the two-mass drivetrain model is shown in Fig. 12. It can be observed that the experimental system is very close to the model and would be proper for our experimental verification. In the settings, the saturation of the pitch angle is properly set as [-5, 25] deg, and the maximum pitch rate is set as 8 deg/s.

An above-rated case considering a wind gust is implemented, as shown in the upper graph of Fig. 13. The wind speed is disturbed by the gust around $t = 10\ s$. In the experiments, the rotational speed ω_G and ω_R are initialized at their rated values. The aerodynamic torque T_R is calculated according to (1) and the torque reference $\tilde{T}_G$ is set constantly at the rated torque value. The rotation speed ω_G is maintained by the blade pitch controller. Fig. 13 shows the response of the blade pitch angle and the generator speed by the two methods. To highlight the results, the blade pitch angle in 6$\sim$22 seconds is augmented, as shown at the upper right corner of the middle graph in

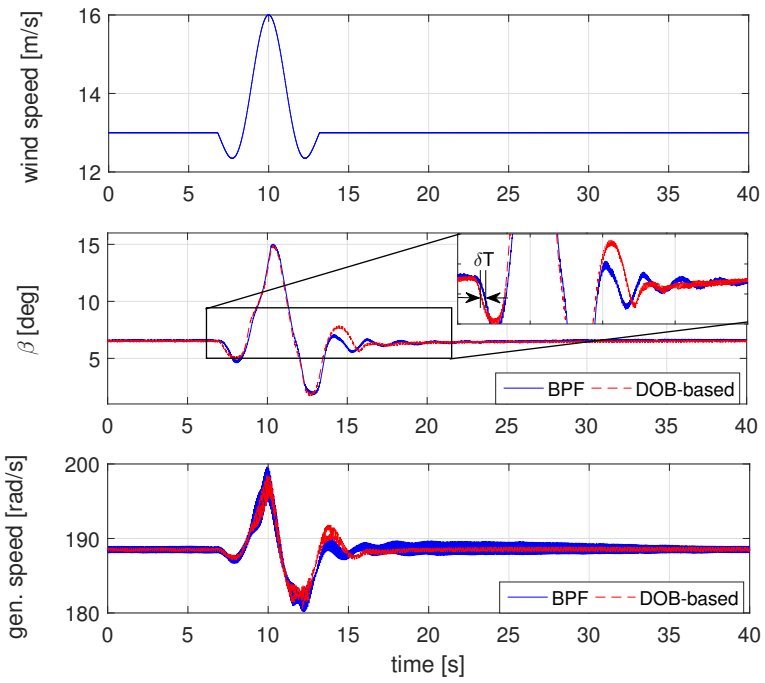

Figure 13: Wind speed (upper graph), blade pitch angle (middle graph) and generator speed (lower graph) in time series.

Fig. 13. Owing to the fact that the sensitivity of the generator speed to the aerodynamic torque is slightly reduced by the BPF, the blade pitch angle responses a little slower ($\delta T \approx 0.2$ s) during the gust. In addition, the blade pitch angle remains oscillation for a longer period (during 13 s$\sim$22 s) after the gust in the BPF method, which means that the performance of the blade pitch controller is deteriorated. Therefore, a retuning procedure becomes necessary for blade pitch controller when the BPF method is applied. From the results, it can also be obtained that a better noise attenuation is achieved by the DOB-based method since the generator speed varies much smoother. Therefore, the effectiveness of the DOB-based method is verified.

6. Conclusion

In this study, a new torsional vibration damper based on disturbance observer has been proposed for variable-speed wind turbines. The filter of the damper was designed by solving a nonlinear optimization problem considering the pole placement of the closed-loop system with model uncertainties. Numerical analysis using a 2-MW wind turbine was applied to illustrate the feasibility of the design method and demonstrate the superior of the damper that not only could the low-frequency gain of the drivetrain system be preserved but also a good noise attenuation performance was obtained. In addition, an experimental system having high consistency with the mathematical model was developed for the hardware-in-the-loop experiment. The experimental results demonstrated the advantage of the damper on preserving the pitch control performance.

Appendix A. DOB-based method for three-mass model

The motion equations of the three-mass system can be expressed by

$$J_1\dot{\omega}_1 + D_1\dot{\theta}_{12} + K_1\theta_{12} = T_R, \tag{Appendix A.1}$$

$$J_2\dot{\omega}_2 - D_1\dot{\theta}_{12} - K_1\theta_{12} = -D_2\dot{\theta}_{23} - K_2\theta_{23}, \tag{Appendix A.2}$$

$$J_3\dot{\omega}_3 - D_2\dot{\theta}_{23} - K_2\theta_{23} = T_G, \tag{Appendix A.3}$$

$$\dot{\theta}_{12} = \omega_1 - \omega_2, \tag{Appendix A.4}$$

$$\dot{\theta}_{23} = \omega_2 - \omega_3, \tag{Appendix A.5}$$

where J_1, J_2 and J_3 are the moment of inertia of the bodies, ω_1, ω_2 and ω_3 are the corresponding rotation speeds. The damping D_1, D_2 and the spring stiffness K_1, K_2 are applied to connect the bodies. The damping terms are ignored during the following analysis.

By calculation, the transfer functions from T_R and T_G to ω_3 are

$$\frac{\Omega_3}{\Gamma_R} = \frac{\omega_a^2\omega_b^2}{J_3 s \cdot P_t(s)}, \tag{Appendix A.6}$$

$$\frac{\Omega_3}{\Gamma_G} = \frac{(s^2+\omega_a^2)(s^2+\omega_b^2)}{J_3 s \cdot P_t(s)}, \tag{Appendix A.7}$$

where $\omega_a^2 = \frac{K_1}{J_1}$, $\omega_b^2 = \frac{K_2}{J_2}$. $P_t(s)$ is

$$P_t(s) = s^4 + \left(\frac{K_1}{J_1} + \frac{K_1}{J_2} + \frac{K_2}{J_2} + \frac{K_2}{J_3}\right)s^2 + \frac{K_1K_2(J_1+J_2+J_3)}{J_1J_2J_3}. \tag{Appendix A.8}$$

By the DOB-based method, Γ_G is expressed by

$$\Gamma_G = \tilde{\Gamma}_G - (J_3 s Q\Omega_3 - Q\Gamma_G), \tag{Appendix A.9}$$

where Ω_3 is the Laplace transfer of ω_3 and Q is the filter expressed by (21) to be designed. The transfer functions become

$$\frac{\Omega_3}{\Gamma_R} = \frac{\omega_a^2 \omega_b^2}{J_3 s} \cdot \frac{1-Q}{P_q(s)}, \quad \text{(Appendix A.10)}$$

$$\frac{\Omega_3}{\tilde{\Gamma}_G} = \frac{(s^2+\omega_a^2)(s^2+\omega_b^2)}{J_3 s} \cdot \frac{1}{P_q(s)}, \quad \text{(Appendix A.11)}$$

where $P_q(s)$ is

$$P_q(s) = P_t(s)(1-Q) + (s^2+\omega_a^2)(s^2+\omega_b^2)Q. \quad \text{(Appendix A.12)}$$

The numerator of $P_q(s)$ can be arbitrarily specified by Q with the degree $n = 5$. The optimization problem considering the pole placement can be formulated in a similar way to (28).

Reference

Bianchi, F.D., de Battista, H., Mantz, R.J., 2007. Wind Turbine Control Systems: Principles, Modelling and Gain Scheduling Design. Springer.

Bir, G., Jonkman, J., 2007. Aeroelastic instabilities of large offshore and onshore wind turbines, in: Journal of Physics: Conference Series, p. 012069.

Bossanyi, E., 2000. The design of closed loop controllers for wind turbines. Wind Energy 3, 149–163.

Bossanyi, E., 2003. Wind turbine control for load reduction. Wind Energy 6, 229–244.

Bossanyi, E., 2015. GH Bladed user manual (version 4.7). Garrad Hassan Bladed .

Boukhezzar, B., Lupu, L., Siguerdidjane, H., Hand, M., 2007. Multivariable control strategy for variable speed, variable pitch wind turbines. Renewable Energy 32, 1273–1287.

Burton, T., Jenkins, N., Sharpe, D., Bossanyi, E., 2011. Wind Energy Handbook. 2 ed., New York: Wiley.

Chen, J., Song, Y., 2016. Dynamic loads of variable-speed wind energy conversion system. IEEE Transactions on Industrial Electronics 63, 178–188.

Cheng, F., Peng, Y., Qu, L., Qiao, W., 2016. Current-based fault detection and identification for wind turbine drivetrain gearboxes. IEEE Transactions on Industry Applications 10.1109/TIA.2016.2628362.

Chilali, M., Gahinet, P., 1996. H_∞ design with pole placement constraints: an LMI approach. IEEE Transactions on Automatic Control 41, 358–367.

Fateh, F., White, W.N., Gruenbacher, D., 2017. Torsional vibrations mitigation in the drivetrain of DFIG-based grid-connected wind turbine. IEEE Transactions on Industry Applications 53, 5760–5767.

Girsang, I.P., Dhupia, J.S., Muljadi, E., Singh, M., Jonkman, J., 2013. Modeling and control to mitigate resonant load in variable-speed wind turbine drivetrain. IEEE Journal of Emerging and Selected Topics in Power Electronics 1, 277–286.

Girsang, I.P., Dhupia, J.S., Muljadi, E., Singh, M., Pao, L.Y., 2014. Gearbox and drivetrain models to study dynamic effects of modern wind turbines. IEEE Transactions on Industry Applications 50, 3777–3786.

Goodwin, G.C., Graebe, S.F., Salgado, M.E., 2001. Control System Design. New Jersey: Prentice Hall.

Hori, Y., Sawada, H., Chun, Y., 1999. Slow resonance ratio control for vibration suppression and disturbance rejection in torsional system. IEEE Transactions on Industrial Electronics 46, 162–168.

Ji, J.K., Sul, S.K., 1995. Kalman filter and LQ based speed controller for torsional vibration suppression in a 2-mass motor drive system. IEEE Transactions on industrial electronics 42, 564–571.

Kambrath, J.K., Khan, M.S.U., Wang, Y., Maswood, A.I., Yoon, Y.J., 2018. A novel control technique to reduce the effects of torsional interaction in wind turbine system. IEEE Journal of Emerging and Selected Topics in Power Electronics .

Licari, J., Ugalde-Loo, C.E., Ekanayake, J.B., Jenkins, N., 2013. Damping of torsional vibrations in a variable-speed wind turbine. IEEE Transactions on Energy Conversion 28, 172–180.

Licari, J., Ugalde-Loo, C.E., Liang, J., Ekanayake, J., Jenkins, N., 2012. Torsional damping considering both shaft and blade flexibilities. Wind Engineering 36, 181–195.

Manabe, S., 2003. Importance of coefficient diagram in polynomial method, in: Decision and Control, 2003. Proceedings. 42nd IEEE Conference on, pp. 3489–3494.

MathWorks, 2020. Optimization toolbox, constrained optimization, fmincon.

Availabe online: http://www. mathworks. com/help/optim/ug/fmincon. html (accessed on 17th August 2020) .

Sariyildiz, E., Ohnishi, K., 2015. Stability and robustness of disturbance-observer-based motion control systems. IEEE Transactions on Industrial Electronics 62, 414–422.

Thore, C.J., 2013. Fminsdp–a code for solving optimization problems with matrix inequality constraints. Freely available at, http://www. mathworks. com/matlabcentral/fileexchange/43643-fminsdp .

Wang, J., Cheng, F., Qiao, W., Qu, L., 2018. Multiscale filtering reconstruction for wind turbine gearbox fault diagnosis under varying-speed and noisy conditions. IEEE Transactions on Industrial Electronics 65, 4268–4278.

Yin, M., Li, G., Zhou, M., Zhao, C., 2007. Modeling of the wind turbine with a permanent magnet synchronous generator for integration, in: Power Engineering Society General Meeting, 2007. IEEE, IEEE. pp. 1–6.

Zhu, H., Fujimoto, H., 2014. Suppression of current quantization effects for precise current control of spmsm using dithering techniques and kalman filter. Industrial Informatics, IEEE Transactions on 10, 1361–1371.

Zhu, H., Yoshida, S., Kajiwara, H., Ogawa, Y., Nakada, S., Ono, J., 2017. A study on torsional vibration reduction for variable-speed variable-pitch wind turbines, in: Mechatronics (ICM), 2017 IEEE International Conference on, IEEE. pp. 318–323.